Translational Diffusion of Paramagnetic Tracers in HEMA Gels and in Concentrated Solutions of PolyHEMA by 1D Electron Spin Resonance Imaging

Antonín Marek, Jiří Labský, Čestmír Koňák, and Jan Pilař*

Institute of Macromolecular Chemistry, Academy of Sciences of the Czech Republic, 162 06 Prague, Czech Republic

Shulamith Schlick

Department of Chemistry, University of Detroit Mercy, Detroit, Michigan 48219

Received January 17, 2002

ABSTRACT: Suitable experimental techniques and theoretical deconvolution and simulation procedures applicable to determination of concentration profiles of paramagnetic particles by ESRI technique and for subsequent determination of diffusion coefficients of paramagnetic tracers in the sample were proposed. The macroscopic diffusion coefficients, D, of paramagnetic tracers in cross-linked 2-hydroxyethyl methacrylate (HEMA) gels equilibrium-swollen with methanol and in polyHEMA methanolic solutions were measured by one-dimensional electron spin resonance imaging (1D ESRI). Both types of the matrix were characterized by dynamic correlation length, L_h, determined by dynamic light scattering (DLS). The dependence of diffusion coefficients on concentration of polyHEMA in methanolic solutions was well fitted within both Phillies' and Petit's models at approximately the same level of accuracy. A slower diffusion of the tracers was found in HEMA gels compared with the solution containing the same concentration of polyHEMA and even with the solution characterized by the same hydrodynamic mean distance between adjacent entanglement points. The results demonstrate the high potential of the 1D ESRI technique and of the data processing methods developed for measurements of diffusion coefficients of paramagnetic tracers in polymer systems.

Introduction

Understanding diffusion processes in swollen polymer networks (polymer gels) and in concentrated polymer solutions has direct impact on numerous practical applications such as drug delivery systems and transport across membranes. Comparison of tracer mobility in gels with that in non-cross-linked polymer solutions can provide important insight into the diffusion mechanism in both situations. Despite numerous data characterizing self-diffusion processes in polymer solutions, a consensus, even in this narrow field, has not been attained yet.[1−3] Data characterizing diffusion of low-molecular-weight tracers in concentrated polymer solutions and especially in gels are comparatively sparse.

Most of the published data characterizing self-diffusion of low-molecular-weight tracers were provided by the pulsed-gradient spin-echo (PGSE) ^{1}H NMR technique. Poly(ethylene glycol)s (PEGs) are suitable tracers for studies of diffusion processes due to their availability in a wide range of molecular weights (from monomer through oligomers up to high-molecular-weight polymers) at very low polydispersity, good solubility in most common solvents, and, the most important for PGSE, good resolution and suitable positions of peaks in the NMR spectra together with long relaxation times. There is also a pronounced tendency of even low-molecular-weight PEGs to associate in very dilute solutions. However, according to numerous dynamic light scattering (DLS) data, the aggregates represent only a small weight fraction of the material in solution. The molecular size of PEGs has usually been characterized by the radius of gyration, R_G, or by the hydrodynamic radius, R_H, measured by static or dynamic light scattering, respectively.[4−6]

Self-diffusion coefficients of PEGs in dilute aqueous solutions measured by PGSE and extrapolated to infinite dilution, D_0, were found[7] to follow Flory's scaling law[8,9]

$$D_0 \sim M^{\alpha_1} \tag{1}$$

surprisingly over the entire molecular weight range studied (from 106 for dimer to 632 000). In eq 1, M is molecular weight of the diffusing polymer molecule, and for the scaling exponent α_1 the excluded-volume model predicts the value $\alpha_1 = 0.6$ in the case of the polymer molecule in a good solvent at sufficiently high temperature. A PGSE study has shown[10] that diffusion coefficients of tracers in aqueous solutions of poly(vinyl alcohol) (PVA) decrease with increasing both the molecular size of tracers and PVA concentration. The dependence of experimental diffusion coefficients of PEGs with molecular weights 400 and 4000 on the PVA concentration in the range 0−0.3 g/mL could be described by a stretched exponential function of the form

$$D = D_0 \exp(-\alpha_2 c^{\nu_2}) \tag{2}$$

resulting from the hydrodynamic scaling model for polymer dynamics proposed by Phillies.[1] The model explicitly assumes that the dominant polymer−polymer forces are hydrodynamic in nature and that entanglement and topological effects provide secondary corrections, in which it differs substantially from the scaling model. The polymer chain contraction at high concen-

* Corresponding author. E-mail: pilar@imc.cas.cz.

10.1021/ma0200874 CCC: $22.00
Published on Web 06/04/2002

trations and the assumption of self-similarity at various concentrations are other basic assumptions. D_0 in eq 2 represents diffusion coefficient of the tracer in neat solvent; α_2 and ν_2 are parameters of the model. The parameter α_2 was predicted to increase as the molecular size (molecular weight) of the tracer increases; the exponent ν_2, which characterizes polymer matrix, was predicted to take a value of 0.5 for matrices formed by long polymer chains or value 1.0 for short ones, and it should vary as $M^{-1/4}$, where M is molecular weight of the PVA, between these limits. The values of both scaling parameters in general agreement with theoretical predictions were determined by fitting experimental diffusion data to eq 2.[10]

The dependence of tracer diffusion coefficients of ethylene glycol, its oligomers, and polymers with molecular weights up to 4000 on the concentration of PVA in aqueous solution ranging from 0 to 0.38 g/mL as determined by PGSE was well fitted[5] to eq 3, resulting from the new physical model for the diffusion of solvents and tracers of Petit et al.[11]

$$D = D_0/(1 + \alpha_3 c^{2\nu_3}) \tag{3}$$

In this model, the polymer solution is regarded as a network where the diffusing molecules have to overcome periodic energy barriers of equal amplitude. The potential barrier is higher for the larger diffusants, and the distance between the barriers corresponds to the correlation length in polymer solution (mesh size). In eq 3 D_0 is the diffusion coefficient of the tracer in the absence of the polymer, $\alpha_3 = D_0/k\beta^2$, and $k\beta^2$ and ν_3 are parameters of the model. The parameter ν_3 depends on the quality of the solvent and should be constant for a given system. Values close to $\nu_3 = 0.58$ were found for the PVA−water system. Parameter β should be a constant independent of the concentration or molecular weight of the polymer matrix; parameter k is the jump frequency, which varies with the molecular weight or size of the tracer. The $k\beta^2$ value was found to depend on the hydrodynamic radius of the tracer calculated from the diffusion coefficients using the Stokes−Einstein equation. Dependences of the diffusion coefficients of water and PEG 600 on the concentration of PVA in aqueous solutions and in some gels were equally well fitted[3] to both eqs 2 and 3. No significant dependence of the diffusion coefficient on the molecular weight of the matrix polymer was observed.

The PGSE technique has also been used[12] for measurement of tracer diffusion coefficients of PEGs of molecular weight ranging from 4250 to 20 000 in poly(*N*,*N*-dimethylacrylamide) gels equilibrium-swollen with D_2O. The gels were characterized by the degree of swelling (Q) defined as the ratio of the mass of swollen polymer gel ($M_{swollen}$) to the mass of dry polymer (M_{dry}), $Q = M_{swollen}/M_{dry}$, and by the density of cross-linking points (N_c) which at equilibrium swelling is related to the degree of swelling by the equation[13] $N_c \approx Q^{-5/3}$. Diffusion data were analyzed on the basis of the ratio of the screening length of polymer network to the size of PEG using the relation

$$D/D_0 = \exp(-\kappa R) \tag{4}$$

suggested earlier for description of diffusion of spherical particles in polymer systems which is based on a modified free volume theory. In this equation, D_0 is the diffusion coefficient of a free isolated particle, R is radius of a particle, and κ^{-1} is the dynamic screening length of polymer chain forming the matrix. In the cases when κ^{-1} is large enough for tracer polymer to show the same motion as a hard sphere rather than the reptational motion, the interchain hydrodynamic interactions more significantly contribute to the diffusion process compared with the topological constrains. For such cases, R can be identified with the hydrodynamic radius of the tracer. When D_0 for PEG is determined from the diffusion coefficient in dilute solution, the change of local friction of the polymer matrix should be taken into account. The relation between κ^{-1} and the concentration of the network polymer c or the degree of swelling Q is expressed by $\kappa^{-1} \sim c^u = Q^{-u}$, where u is a constant in the range from −0.5 to −1.0 depending largely on the polymer species. Fits of the experimental data to eq 4 over the Q range from 5 to 50% have shown[12a] proportionality of the dynamic screening length κ^{-1} to $c^{-0.71}$.

Electron spin resonance imaging (ESRI) has emerged as another powerful tool for measuring macroscopic diffusion coefficients of paramagnetic tracers in various matrices. Since ESRI was comprehensively reviewed,[14] new applications of particularly one-dimensional (1D) X-band ESRI to such measurements in various systems were reported.[15−18] In principle, the experimental concentration profile of the paramagnetic tracer in a sample can be determined from ESRI experimental data taken at particular time after the start of diffusion by a suitable deconvolution procedure. By fitting the theoretical concentration profile of the tracer in the sample, expressed as a solution of Fick's equation for proper sample configuration, to the experimental profile, the diffusion coefficient as one of the parameters of the fit can be deduced.

In one of our previous papers[19] we have used two-dimensional (2D) spectral-space ESRI for studies of the macroscopic diffusion coefficients of paramagnetic tracers in HEMA−DEGMA hydrogels. The gels were prepared by copolymerization of 2-hydroxyethyl methacrylate (HEMA) (**I**) (Chart 1) and 2-(2-hydroxyethoxy)ethyl methacrylate (DEGMA) in the presence of the cross-linker (**II**) and equilibrium-swollen with water. Data in reasonable agreement with some theoretical models were obtained. Diffusion in polymer gels in the equilibrium swelling state was studied in order to eliminate the contribution of the concentration gradient of the solvent to the driving force governing tracer diffusion. A similar study revealed[20] a slower diffusion of the low-molecular-weight paramagnetic tracer 4-oxo-3,3,5,5-[$^2H_4$]-2,2,6,6-tetra([$^2H_3$]methyl)piperidin-1-yloxyl (**IV**) in a polystyrene network (chemically cross-linked gel) swollen with toluene when compared with a toluene solution containing the same volume fraction of linear polystyrene. These findings[21] encouraged us to focus our attention on the investigation of the effect of permanent chemical cross-links in gels on diffusion coefficients of tracers. Such cross-links, which are responsible for mechanical properties of gels, are present in the gel in addition to the temporary entanglements existing in solution. In the next step we have decided to use the 1D ESRI technique, which enables faster and more precise determination of macroscopic diffusion coefficients, instead of extremely time-consuming redundant 2D spectral-space ESRI. We have used 1D ESRI for measurement of diffusion coefficients of paramagnetic tracers in lightly cross-linked poly(1-vinyl-2-pyrrolidone) (PVP) hydrogel (equilibrium water content 88 wt %) and

Chart 1

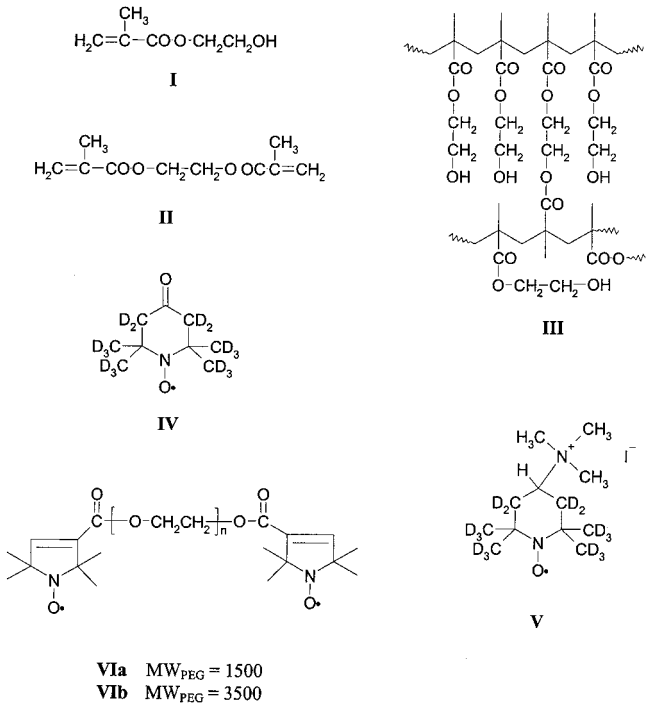

in aqueous solution of PVP containing the same polymer volume fraction.[22] In this case convolution of the theoretical concentration profile of the tracer in the sample with the ESR spectrum of the sample taken in the absence of the gradient was fitted to the ESRI projection using a least-squares-fitting program based on a minimization algorithm. The best-fit diffusion coefficients determined clearly indicate that even small concentrations of permanent cross-links in the lightly cross-linked PVP gel are able to reduce the rate of transport of a bulky paramagnetic tracer to the value corresponding to a higher volume fraction (2-fold) of linear PVP in solution, where no fixed obstacles (permanent cross-links) are present.

In the present study of diffusion of paramagnetic tracers in polyHEMA methanolic solutions and in HEMA gels swollen with methanol, we have employed the 1D ESRI technique and suitable deconvolution procedures for determination of the experimental concentration profiles of the tracers in samples. In the fitting process aimed at determination of diffusion coefficients of particular tracers, systematic deviations of the experimental concentration profiles from those predicted by theory were found. This made us modify both experimental arrangement and computational techniques so that the deviation between the experimental and theoretical profiles is minimized. The experimental procedure and software capable of analyzing experimental data measured in various experimental arrangements and the corresponding basic theory are briefly described below. Methanol was used as solvent in this study due to insolubility of polyHEMA in the previously used[19] water.

Experimental Section

The experiment consists of the following steps: (1) sample preparation and characterization, (2) 1D ESRI measurement in the course of diffusion, (3) determination of the tracer 1D concentration profiles by a deconvolution procedure, (4) estimation of the diffusion coefficient by fitting the experimental to theoretical tracer 1D concentration profile calculated using a proper solution of Fick's equation.

Table 1. Characterization of Polymer Solutions (S) and Gels (G) Used in Diffusion Studies

sample code	cross-linker c_c (wt %)	polyHEMA c_H (wt %)	polymer c (g/mL)]	$\Phi^2 \times 10^3$	L_H (nm)	Q^d
G23	0.7	23	0.201	158	6.7[b]	4.32
G29	3.5	29	0.255	200	4.1[b]	3.48
G35	3.8	35	0.323	254	3.2[b]	2.83
S02		0.2	0.00158	1.24	10.3[c]	
S05		0.5	0.00396	3.11	10.5[c]	
S1		1	0.00794	6.23	10.3[c]	
S2		2	0.0159	12.5	10.4[c]	
S5		5	0.0403	31.6	10.6[c]	
S10		13	0.0822	64.5	9.8[c]	
S23		23	0.199	156	6.9[b]	
S29		29	0.258	202	6.0[b]	
S35		35	0.319	251	5.1[b]	
S50		50	0.488	383	2.9[b]	

[a] Polymer volume fraction. [b] Hydrodynamic correlation length determined by DLS in gels and in nondilute solutions. [c] Hydrodynamic radius R_H determined by DLS in dilute solutions. [d] Degree of swelling of the gel calculated form the composition of the polymerization mixture.

Materials. Methanolic solutions of poly(2-hydroxyethyl methacrylate) (polyHEMA) were prepared by dissolving proper amounts of commercial polymer (Polysciences Inc.) in a closed vessel until homogeneous, highly viscous solutions were obtained. Gel chromatography performed in dimethylacetamide using polystyrene standards showed $M_w \sim 1000\,000$ and a very high polydispersity (>4) of the polymer. Static light scattering measurement (SOFICA 42 000) in methanol yielded $M_w \sim 960\,000$ and $R_G < 30$ nm. Such a small radius of gyration at a relatively high molecular weight of the polymer indicates both the presence of branching, which is usual for poly(HEMA) due to the presence of nonremovable amount of cross-linker (**II**) in the polymerization mixture, and low thermodynamic quality of methanol for polyHEMA.

HEMA gels (**III**) (Chart 1) were prepared by polymerization of a mixture of 2-hydroxyethyl methacrylate (**I**) (containing a nonremovable amount of 0.12% of ethylene dimethacrylate cross-linker as determined by gas chromatography), ethylene dimethacrylate cross-linker (**II**), 2,2′-azobis(2-methylpropanenitrile) initiator (Fluka), and methanol in proper proportions (Table 1). After 10 min bubbling with argon the mixture was filled into glass capillary tubes (i.d. about 1 mm) and into larger glass ampules (i.d. about 10 mm) in the case of ESRI and other samples (light scattering and swelling), respectively. Capillaries and ampules were sealed up and the reaction mixture was polymerized at 65 °C for 8 h. Some larger (10 mm) samples from each series were subjected to a swelling test first. The gel was removed from the ampules and immersed into excess of methanol. Swelling was monitored by weighing the sample until equilibrium was reached. The procedure was repeated several times using a corrected composition of the polymerization mixture, and as a result of the iterative procedure, three types of gels polymerized in the presence of an amount of methanol required for equilibrium swelling of the particular gel composition were prepared (Table 1) in the final step. Degrees of swelling Q were calculated using $Q = M_{swollen}/M_{dry}$ where $M_{dry} = m_{cross-linker} + m_{HEMA}$ and $M_{swollen} = M_{dry} + m_{MeOH}$. The selected gels were used for light scattering and ESRI experiments as described below.

The synthesis of paramagnetic tracers used in the study (**IV**−**VI**) (Chart 1) was described[19,22] earlier. The tracers **VIa,b** were characterized by MALDI−TOF mass spectrometry (Biflex III, Bruker Daltonik, Bremen, Germany). Solutions of a sample, a dithranol (anthracene-1,8,9-triol) matrix, and a cationizing agent (sodium trifluoroacetate) in tetrahydrofuran were prepared at concentrations 10 mg/mL and mixed in the ratio 40:10:1. One microliter of the mixture was deposited on the sample plate and air-dried. The spectra were collected in the reflectron mode (Figure 1). For both tracers, the spectra

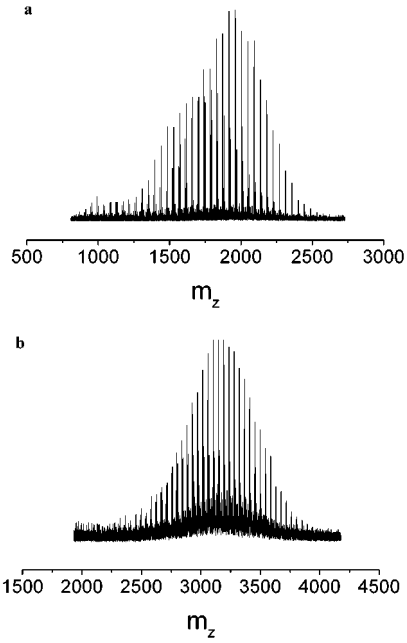

Figure 1. MALDI−TOF mass spectra of tracers **VIa** (a) and **VIb** (b).

consist of two series of peaks: one corresponding to chains labeled at one end only and the other to chains labeled at both ends; there is no indication of unlabeled chains. The results obtained by analysis of the spectra of each tracer made both for each of the series separately and for both series together showed very low polydispersity. Molecular weights $M_w/M_n =$ 1840/1800 for tracer **VIa** and $M_w/M_n = 2920/2900$ for tracer **VIb** were determined. For both samples the difference in molecular weight of the observed series is close to the molecular weight of the label and thus corroborates the assignment of peaks. Comparison of total areas under the peaks in each series indicates that more than 80% of hydroxy end groups in functionalized PEG standards were successfully labeled in both types of samples.

Sample Characterization by Dynamic Light Scattering (DLS). Gel samples polymerized in glass ampules and polyHEMA solutions filled into the ampules were used for DLS experiments. Polarized DLS measurements were made at a scattering angle of 90° using a light-scattering apparatus equipped with an argon laser (514.5 nm) and an ALV 5000, multibit, multitau autocorrelator covering approximately 12 decades in the delay time. To avoid an effect of nonergodicity of gel samples on the dynamic light scattering results, the samples were rotated, and intensity autocorrelation functions obtained by averaging at least 10 measurements at different sample positions were used for analysis. The correlation functions were analyzed with the REPES program,[23,24] which targets the inverse Laplace transformation. The collective (cooperative, gel mode) diffusion coefficients, D_c, of concentrated solutions and gels were calculated in standard way from the mean characteristic decay times using the expression $D_c = 1/\tau_c q^2(1-\Phi)^2$, where τ_c is the mean characteristic decay time, $q = 4\pi n_0 \sin(\theta/2)/\lambda_0$ is the magnitude of the scattering vector, n_0 is the refractive index of the solvent, and λ_0 is the wavelength of the incident light. In this expression, a correction for solvent back-flow[25] is included, by division by $(1-\Phi)^2$, where Φ is the polymer volume fraction ($\Phi = \bar{\nu}_2 c$, $\bar{\nu}_2 = 0.785$ cm^3 g^{-1} is the partial specific volume[26] of polyHEMA and c, g/mL, is the polymer concentration). D_c for gels was further corrected by the heterodyne method introduced by Geissler.[27] Then the concentrated polymer solutions and gels were characterized by the dynamic correlation length, L_H, by using the Stokes−Einstein relation, $L_H = kT/6\pi\eta D_c$, where T is the absolute temperature, k is the Boltzmann constant, and η the viscosity of the solvent. The L_H is identified with hydrodynamic radius, R_H, in dilute solutions and with dynamic correlation length (hydrodynamic blob size), ξ_H, in entangled solutions (pseudogel regime) and in gels. In the case of polymer gels, the DLS technique is not able to resolve contribution of temporarily entanglement points and permanent cross-links to ξ_H. The L_H was determined with accuracy better than 5% in polymer solutions and better than 10% in polymer gels.

ESRI Samples Preparation and Measurement. For ESRI measurements, methanolic solutions of linear poly(HEMA) were filled into glass capillaries of i.d. ≈1 mm and HEMA gels were polymerized inside. The lengths of the samples ranged from 3 to 10 mm. The diffusion was started with approximately 0.2 μL of 5×10^{-2} M methanolic solution of a paramagnetic tracer. For short-time diffusion (<1 h), the capillary was closed with Parafilm; for longer experiments it was necessary to seal the upper end of the capillary in order to prevent the surface of the polymer matrix (either gel or solution) from drying due to evaporation of the volatile solvent. In the empty space between the polymer and upper seal, cotton soaked with methanol was placed to saturate the vapor phase. The capillary was then inserted into an ESR quartz sample tube (4 mm o.d.) and placed, with its axis parallel to the gradient direction, in the cavity of the ESR spectrometer.

Because the gel samples were already polymerized in the capillary, the tracer solution in this case simply topped the gel ("from-top-to-bottom" arrangement). Two other experimental arrangements that require careful manipulation were also used for measurements in polymer solutions. A small drop of the tracer solution was put on the bottom of the capillary, and the diffusion was started by overlying it with the polymer solution ("from-bottom-to-top" arrangement). The third arrangement is a combination of both. The diffusion was started just as in the "from-top-to-bottom" arrangement, but then the tracer was overlayered with the polymer solution ("sandwich" arrangement). Crucial for the choice of arrangements are the requirements for (a) preservation of the uniformity of the diffusion in the sample cross-section along its active length so that the 1D solutions of Fick's law could be applied, (b) preservation of the sample for a long time, and (c) easy manipulation. Generally, the "sandwich" arrangement provides the data that could be precisely analyzed, the "from-top-to-bottom" arrangement is easy to carry out, and the "from-bottom-to-top" arrangement is sometimes a reasonable compromise. During the sample preparation, care must be taken to prevent the surface of the polymer matrix (either gel or solution) from drying due to evaporation of the volatile solvent.

The ESRI system in the Detroit laboratory consists of a Bruker 200D ESR spectrometer with an EMX console, equipped with two eight-shaped Lewis coils fed by two regulated power supplies. Measurements were performed using a vertical gradient (perpendicular to the external magnetic field); $G_{max} \approx 250$ G/cm. The instrumentation has been described in more detail elsewhere.[19−22] All the measurements were performed at the temperature inside the cavity of the ESR spectrometer stabilized at 300 ± 1 K, and the samples were kept at the same temperature when outside the cavity.

For determination of the 1D concentration profile of the tracer at a particular time after starting the diffusion, an ESR projection of the sample in the presence of the gradient field and its ESR spectrum in its absence at a particular time must be measured. We have measured spectrum-projection pairs at several suitable times after starting the diffusion for each of the samples to be able to estimate experimental error and to disclose possible effects of non-Fickian processes characterized by time-dependent diffusion coefficients. The effect of the gradient magnitude on the quality of the data was tested by using various gradients (50−150 G/cm) for most of the samples.

Data Analysis

Determination of Experimental Concentration Profiles by Deconvolution Techniques. The ESR spectrum measured in the presence of the gradient (projection) could be expressed as a superposition of the spectra of all individual tracers at various positions

inside the sample (i.e., at various effective external magnetic fields) weighted by the spectrometer sensitivity at a particular position. Providing that there is no line shape variation in the ESR spectrum of the tracer throughout the sample, such a projection could be mathematically expressed as a convolution of the spectrum measured at the gradient-off and the concentration profile of the tracer inside the sample multiplied by the spatial sensitivity function of the spectrometer.[28] The sensitivity function could be readily determined by measuring concentration profile in the sample with homogeneous tracer distribution. To get the concentration profile, we need to perform the reverse deconvolution process, i.e., to deconvolute the spectrum at the gradient-off out of the projection measured at the gradient-on. If the spatial region of the diffusion is wide (>5 mm), it is necessary to divide the result of the deconvolution by the spectrometer spatial sensitivity function.

Deconvolution is a well-known numerical problem, and many deconvolution methods have been developed so far.[29] In matrix representation, we may write in a discrete case a convolution of vectors $i = s*o$ as $i_n = s_{nm}o_m$, where i_n, s_n, and o_n are discrete spectra measured at the gradient-on and -off and the tracer concentration profile, respectively, and the elements of matrix s_{nm} are given by $s_{nm} = s_{n-m}$. A naive approach to the deconvolution is to solve the set of linear equations in unknowns o_m by using the inverse matrix $o_m = s_{nm}^{-1}i_n$. Because of noise perturbations, which are always present in any physical measurement, the solution o_m typically exhibits large spurious fluctuations. Another linear method is based on the Fourier convolution theorem, which states that the convolution of two spectra is a simple multiplication in the Fourier domain. Convolution integral that also respects the additive noise $n(x)$ in the $i(x)$ function and $i(x) = \int_{-\infty}^{+\infty} o(x')s(x - x')x' + n(x)$ could be simplified in the Fourier domain as $I(\omega) = O(\omega)S(\omega) + N(\omega)$. By dividing this equation by $S(\omega)$ and solving for $O(\omega)$, we get $O(\omega) = I(\omega)/S(\omega) - N(\omega)/S(\omega)$ and inverse transformation would produce the restoration of $o(x)$. The noise term in this equation, however, is predominantly random, increasing with frequency and, for higher noise levels, spurious high-frequency fluctuations obscure all the information in the deconvoluted results.

Fluctuations could be suppressed by band limiting. We may set a frequency cutoff Ω for the estimate o and separate the low-frequency information. However, the spectral structure beyond the cutoff is lost, and the estimate is somehow smeared. Only deconvolution methods that utilize some prior knowledge of the estimate are able to restore to a certain extent the "lost" frequencies beyond the cutoff. Below we will describe two constrained nonlinear methods used in this study. The term "nonlinear" describes the situation in which the solution o cannot be expressed as a linear function of the i. By the word "constraint", we mean physically meaningful bounds placed on the concentration profile as the solution. We require the concentration profile be positive (positivity or minimum negativity constraint), nonzero only over a certain limited region (finite extent constraint), and, finally, also smooth.

The first nonlinear deconvolution method used extends the approach based on the Fourier analysis by implementing constraints. We use a Matlab Signal Processing Toolbox to create digital low-pass filters of various types and sampling, pass-band, and stop-band frequencies.[30] We may consider a suitable filter as a smoothness constraint. However, this is done at the expense of sharpness that is lost as the amplitudes of high frequencies are suppressed or cut off. Howard described a technique that is partly capable of restoring amplitudes of frequencies beyond the cutoff (Fourier spectrum continuation).[31−33] He has shown how to formulate mathematically the finite extent and minimum negativity constraint as a minimization problem in order to obtain the unknown amplitudes and suggested an iterative procedure for solving a set of nonlinear equations applicable in the case of minimum negativity constraint. Easy accommodation of other constraints (including the finite extent constraint) with only slight modification is the main advantage of this approach. Applying both constraints simultaneously produces a result much more likely to be correct than would be the result of applying each constraint separately.

The second deconvolution method used is based on the construction of an objective function that can be minimized to obtain a best estimate and on the Monte Carlo minimization procedure.[29b] The objective function may use a least-squares criterion as a measure of goodness of the fit and be written as $\Phi(v) = |i - i_M(v)|^2$, where $i_M(v)$ is a model fit based on a set of parameters v. We seek the v parameters that minimize $\Phi(v)$, thereby ensuring the best fit. The model spectrum $i_M(v)$ is further given by the convolution of the model concentration profile and the true spectrum measured at gradient-off $i_M(v) = s*o_M(v)$. The most general case is to take the value of each sampled element of the estimate o_M as a parameter of the objective function and hence the solution. Excessive computation is then required, and the probability of finding only local minima of the objective function Φ is high. Nevertheless, the optimization idea was teamed with a Monte Carlo technique with a proper decision rule. In the Monte Carlo optimization process are accepted or rejected random small changes at each sampled position of o_M. To avoid the local minimum trapping problem, we have to accept with a certain probability also changes that temporarily rise the objective function Φ. However, such probability is gradually lowered until the "frozen" state. This algorithm has a parallel in a physical process called annealing, the process by which the temperature of a system is gradually lowered until its parameters freeze into their final values. Constraints are implemented very simply. A change is rejected whenever it would give rise to a violation of the constraints. Thus, we generate changes only within a region limited by the finite extent constraint, and the changes that would produce negative values of the concentration profile are rejected. The smoothness constraint was implemented by smoothing with a cubic spline after each annealing step.[34]

Whereas positivity and finite-extent constraints are definite bounds in both mentioned methods, the formulation of the smoothness requirement is ambiguous. A rigorous approach to seeking the unique solution with desired features is Frieden's method of maximum likelihood.[29b,35] Unfortunately, even its simple form, the maximum entropy method, has been found virtually inapplicable to our case due to the extremely high computer time required.

Estimation of the Diffusion Coefficient by Fitting the 1D Tracer Concentration Profile. On the assumption that the concentration of the tracer inside

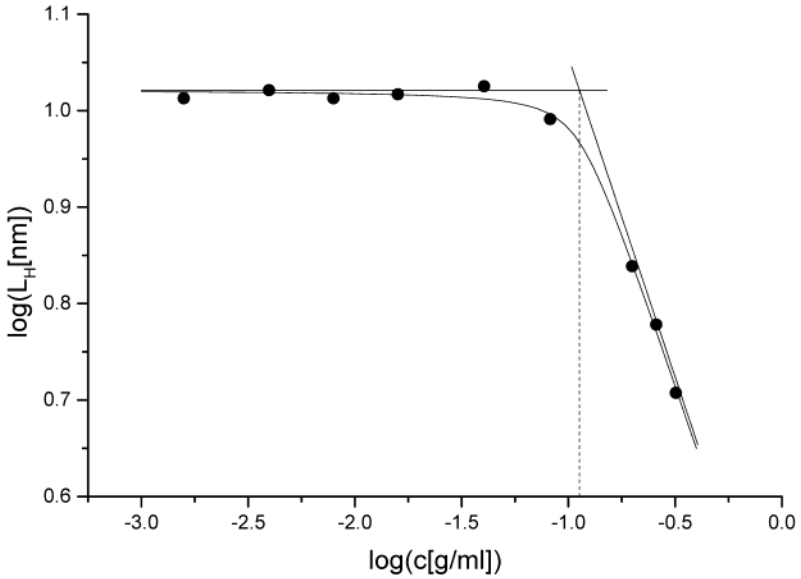

Figure 2. Concentration dependence of dynamic correlation length L_H of polyHEMA in methanolic solution determined by DLS. The dashed line indicates $c^* = 0.11$ g/mL.

the sample is low enough so that the translational diffusion obeys Fick's law $\partial C(\vec{\mathbf{r}},t)/\partial t = D\Delta C(\vec{\mathbf{r}},t)$, and if the diffusion along the capillary axis strongly predominates over those in other directions, we can write the solution of this equation as 1D spatial and time dependence of the tracer concentration

$$C(x,t) = \frac{1}{(4\pi Dt)^{1/2}}\int_{-\infty}^{+\infty} e^{-(x-x')^2/4Dt} C(x',t=0)\, dx'$$

where D is a diffusion coefficient and x is a space coordinate along the gradient direction for an arbitrary initial tracer distribution.[36] If the initial tracer distribution can be described by the delta function, the solution has the form of Green's function, $C(x,t) = G(x,t) = (1/4\pi Dt)e^{-x^2/4Dt}$. After implementation of boundary conditions for the case of reflecting walls at the top surface of the polymer sample and at the bottom of the capillary $\partial C/\partial x|_{x=0,x=L}$, where L is the length of the sample, the solution can be written as

$$C(x,t) = [G(x,t) + \sum_{n=1}^{+\infty} G(2nL - x,t) + G(2nL + x,t)]^* C(x,t=0) \quad (5)$$

where n is the number of reflections on the walls (convergence was reached for $n \leq 3$ in all our calculations). Sometimes it is possible to define mathematically a common initial condition, e.g., the initial distribution of spin probe is close to the δ function or to the layer of a certain width, and then the solution can be expressed in an analytical form.

Once we have found a time series of concentration profiles of the tracer in the sample, it is advantageous to take an early profile as the starting profile for a later one. If the diffusion follows Fick's law, combinations of different pairs of concentration profiles should give the same diffusion coefficient. The plot of Dt vs t could be fitted with a straight line crossing the origin, and its slope gives coefficient D.

For deconvolution and fitting procedures we used Matlab software. Here we benefit from the naturally matrix oriented programming language and plenty of predefined mathematical and graphical routines. For the calculations of the 2D diffusion in the precision test, which will be discussed later, we have used a Matlab-based product Femlab which is an environment for the technical and physical simulations in 1D, 2D, and also 3D space.

Results and Discussion

Sample Characterization. The hydrodynamic correlation lengths, L_H , determined for gels and solutions studied by DLS are given in Table 1. The crossover concentration at which the overlap of the polymer coils begins, c^*, was estimated from the concentration dependence of the characteristic hydrodynamic length L_H of polyHEMA solutions in transition region. The log−log plot of experimental data is shown in Figure 2. The data were fitted to a hyperbolic function having one of the asymptotes parallel to the x axis

$$y = a - (m/2)\{x + [(x - x_0)^2 + d^2]^{1/2}\}$$

where $y = \log L_H$ and $x = \log c$. Coordinates of the intercept of asymptotes are x_0 and $y_0 = a - mx_0/2$, m being the slope of the oblique asymptote and d the distance between the intercept of asymptotes and hyperbolic function along the vertical axis. Since R_H should asymptotically approach its value at zero concentration and ξ_H should follow a power-law dependence on concentration (a linear dependence in log−log plot) in semidilute solutions (at concentrations above c^*), it is plausible to assume that the intercept $x_0 \approx \log c^*$. The values $x_0 = -0.95$ and $c^* = 0.11$ g/mL were determined using the data presented in Figure 2. A significantly higher c^* was found for polyHEMA in methanol when comparing with linear polymers of similar molecular weights in good solvents (e.g., for polystyrene in good solvents c^* lower by more than an order of magnitude was found at similar M_w[37,38]). The high c^* together with the above-mentioned very small R_G found for polyHEMA in methanol by static light scattering indicate that (i) methanol is not a thermodynamically good solvent for polyHEMA and/or (ii) polyHEMA is partly branched. This means that effective

lengths of polyHEMA chains are shorter than that of a hypothetical linear chain and onset of entanglements starts at higher polyHEMA concentrations. The slope of a high-concentration asymptote in Figure 2 gave $u = -0.66$, which lies within the theoretically predicted limits[9] from -0.5 to -1.0.

It follows from Table 1 that ξ_H found in concentrated polyHEMA solutions is systematically larger than ξ_H in gels containing the same polymer volume fraction Φ. This means that the hydrodynamic screening is more intensive in gels than in corresponding solutions and that permanent cross-links play a significant role. Since the hydrodynamic correlation length in concentrated solutions is a measure of the distance between entanglements (the blob size), we can conclude that the distance between entanglements in gels decreases, when compared with corresponding solutions, due to the presence of permanent cross-links.

Diffusion Coefficients. Measurements of diffusion coefficients of paramagnetic tracers in gel samples were performed using the "from-top-to-bottom" arrangement only. All the three mentioned arrangements were used when measuring diffusion coefficients in concentrated solutions. The more elaborated "sandwich" arrangement produces best results because the diffusion region is safely protected by surrounding layers and thus protected from drying due to undesirable evaporation of methanol from the surface of the sample. Such a protective feature provides also the "from-bottom-to-top" arrangement. Another advantage of the sandwich arrangement is the simple Gaussian shape of the concentration profile. The absence of sharp edges in the profile results in a fast decay of amplitudes of its Fourier transform with increasing frequency. Thus, a substantial part of the Fourier transform of the concentration profile is well separated from the high-frequency noise and preserved after filtering. Finally we do not need to care much about reflections discussed below.

Deconvolution of the experimental data was performed using the above-mentioned Fourier method in the first step. The result was used as the starting point for the second mentioned Monte Carlo method, which was used as a feedback to ensure the reverse validity of the convolution relation between the measured spectra and a concentration profile.

An approximation of the diffusion in the samples studied by the 1D free diffusion is expected when analyzing the experimental data. Although the capillary is thin and symmetric, the finite diameter causes a problem in 1D approximation. The initial layer containing the tracer could be nonuniform in the direction perpendicular to the capillary axis. This may be caused by the meniscus at the polymer surface when performing "from-top-to-bottom" diffusion or by smearing the initial layer when trying to overlay it by the polymer sample in the case of the other two arrangements used. Both meniscus and the smear of initial layer result in a nonzero concentration gradient in the direction perpendicular to the capillary axis. This causes a particular problem when fitting a theoretical concentration profile to the experimental one. Because of nonplanarity of the sample surface, the real walls are not sharp as assumed, which implies that the real 1D concentration profile is not terminated by a jump change at the walls but rather by a gradual decrease. The position of the reflection walls is one of the parameters of the fitting procedure. The minimization procedure tries to place the edge of the theoretical concentration profile somewhere in the middle of the broadened slope of the walls of the experimental concentration profile, but this decreases the quality of the fit. The diffusion should be treated as a 3D problem which is practically insolvable because the 3D geometry of the samples is either difficult to describe or unknown.

To overcome this fitting problem, we suggest a symmetrization procedure as a way of minimizing the surface nonplanarity effect. The procedure is based on a semiempirical trick that eliminates the starting wall. Let us assume having a perfect 1D single-directional diffusion that has a sharp wall at its start. We can imagine the same single-directional diffusion but in the opposite direction. The way of elimination of the starting wall is to identify starting walls of both diffusions so that the starting walls overlap. Such symmetrization produces a two-directional diffusion with the same diffusion coefficient. Experimental concentration profiles with broadened walls were subjected to a symmetrization procedure, and a new parameter, the distance between origins of the experimental profile and its mirror image, d, was introduced as variable of the fitting procedure. The origin of every concentration profile is the center of the spatial dimension of the spectral−spatial window in which the deconvolution procedure takes place and the mirror image is mirrored around this point. Because we use experimentally estimated initial conditions, we need to perform the symmetrization procedure with both the final and the initial concentration profile. The resulting nearly Gaussian symmetrized profiles were fitted by theoretical solution (5) with a substantially higher correlation compared with nonsymmetrized profiles. For estimation of the quality of the fit, we have used the standard least-squares criterion.

To determine the error of such procedure, we decided to construct a model diffusion experiment for two arrangements (Figure 3). 2D diffusion for the "sandwich" arrangement in a rectangular capillary 5×1 mm, which are typical measures of our experimental capillaries, was numerically modeled with a single diffusion coefficient $D_{2D} = 2.083 \times 10^{-6}$ cm^2/s using Femlab. As an initial layer, we took a layer of the width 0.5 mm symmetrical around the center. Concentration profiles were generated after 25 and 40 min diffusion. Profiles were integrated along the direction perpendicular to the capillary axis into 1D profiles and then fitted by the standard procedure used for the experimental profiles. The diffusion coefficient $D_{1Da} = 2.080 \times 10^{-6}$ cm^2/s was determined. The agreement between D_{1Da} and D_{2D} demonstrates self-consistency of the numerical algorithms used (Figure 3a). In the next step the capillary was divided into two parts by a flat cut along the diagonal of the initial layer, and 2D diffusion was numerically modeled in a single part only in a manner similar to the case of the whole capillary. The profiles were integrated along the direction perpendicular to the capillary axis into 1D profiles again. Using the symmetrization procedure for determination of the model concentration profile, the fitting process then gave the diffusion coefficient $D_{1Db} = 2.092 \times 10^{-6}$ cm^2/s (Figure 3b). The relative error around 0.5% resulting from comparison of both model diffusion coefficients is more than satisfactory with respect to other experimental errors and to the fact that the length 0.5 mm of the 2D surface effect is overestimated. A typical initial broad-

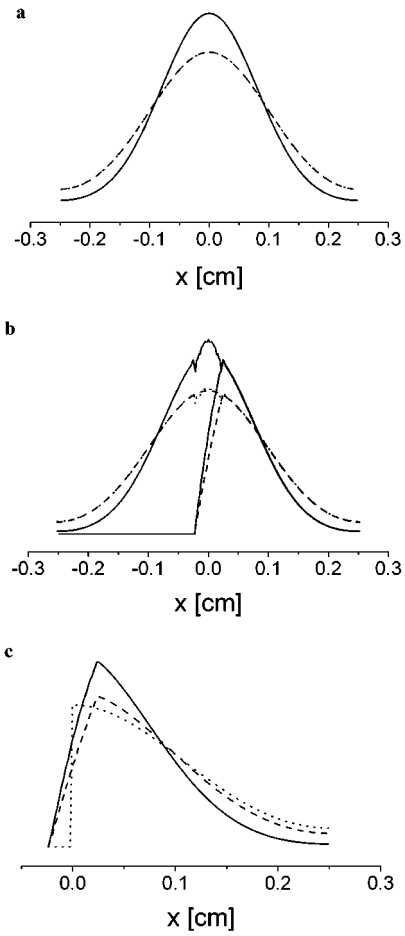

Figure 3. Precision test of the symmetrization process (see the text): (a) 1D concentration profiles calculated from model 2D diffusion in "sandwich" arrangement with $D_{2D} = 2.083 \times 10^{-6}$ cm^2/s at $t_1 = 25$ min (initial profile − full line) and $t_2 = 40$ min (final profile − dashed line); the best fit of eq 5 fits the final profile (dotted line) perfectly and gives the diffusion coefficient $D_{1Da} = 2.080 \times 10^{-6}$ cm^2/s. (b) 1D single-directional concentration profiles calculated as in (a) but only for diffusion into the right half of the 2D model sample, created by the flat cut along the diagonal of the initial layer in order to simulate the surface effect, and the corresponding profiles after symmetrization. The best fit of eq 5 to the final symmetrized profile (dotted line) gave the diffusion coefficient $D_{1Db} = 2.092 \times 10^{-6}$ cm^2/s. (c) Initial and final single-directional concentration profiles from (b) and the poor best fit of eq 5 to the nonsymmetrized final profile (dotted line) which gave diffusion coefficient $D_{1Dc} = 2.902 \times 10^{-6}$ cm^2/s.

ening around 0.3−0.4 mm was observed in real 1D profiles. A much higher value of the diffusion coefficient $D_{1Dc} = 2.902 \times 10^{-6}$ cm^2/s was determined when fitting nonsymmetrized model profiles (Figure 3c). This discrepancy documents the efficiency of the symmetrization method that helps to fit concentration profiles better and to get a more correct value of the diffusion coefficient also in the case when deviations from the theoretical assumptions discussed above occur. The central part of symmetrized profiles exhibit some oscillations, but the overall fit is good. On the other hand, the simulation of the nonsymmetrized profile in Figure 3c is not able to cope with the broadened front edge.

Figure 4 shows examples of experimental data and their processing. In column 1 data for diffusion of tracer **VIa** in sample S30 measured in "sandwich" arrangement in both up and down directions and in column 2 data for downward diffusion of the same tracer in sample S40 in "from-top-to-bottom" are given. In the first row (Figure 4a), initial and final ESR profiles taken at the gradient-on together with the spectrum taken at the gradient-off in the inset are presented. In the second row (Figure 4b), corresponding concentration profiles determined by deconvolution, in the case of the single-directional diffusion (column 2) also symmetrized profiles, and their fits by eq 5 are given. Third row (Figure 4c) shows the dependence of $D\Delta t$ vs Δt for different initial−final profile pairs. The linearity of these dependences proves the time independence of the diffusion coefficients determined, which indicates Fickian diffusion in all the samples studied. The slope of the linear dependence determines the diffusion coefficient for particular tracer and sample.

Macroscopic translational diffusion coefficients D for tracers **IV**, **V**, and **VI a,b** (Chart 1) in polyHEMA solutions and HEMA gels measured by ESRI technique are given in Table 2. Each diffusion coefficient was determined from measurements of typically 2−3 different samples of the same kind of polymer solution or gel. Measurements at typically 6−10 different times after the start of the diffusion were performed, and the diffusion coefficient D for a particular sample was calculated from the slope of the $D\Delta t$ vs Δt dependence. At least two different experimental arrangements (see above) were used when measuring diffusion of a particular tracer in each of polyHEMA solutions. The values D presented in Table 2 are the averages of the values determined for a particular tracer−matrix pair. There are two main contributions to the experimental error of their determination. The error associated with determination of D for a particular sample due to inaccuracies of deconvolution and fitting processes was estimated not to exceed 2%. The accuracy of determination of D from the slope of $D\Delta t$ vs Δt dependences, to which sample drying and similar time-dependent processes could contribute, confirms such estimate. The largest contribution to the error of the average D values presented in Table 2 is due to the unsatisfactory reproducibility of the gel samples mainly, which is in particular due to volatility of the solvent used. The error was estimated to be typically 5 and 10% but did not exceed 10 and 20% for polyHEMA solutions and HEMA gels, respectively. In general, diffusion coefficients of the tracers in polyHEMA methanolic solutions decrease with increasing molecular weight of the tracer. We gave up looking for a more specific character of the dependence with regard to both the number and limited range of molecular weights of the tracers used. A similar dependence follows from the presented diffusion coefficients of the tracers in HEMA gels. The virtually equal coefficients for tracers **VIa** and **VIb** in the matrix G23 are probably due to the accumulation of experimental errors in opposite directions.

Dependence of Diffusion Coefficients on the Matrix Properties. To get information on the effect of temporary entanglements and permanent cross-links present in matrixes, we have analyzed the data presented in Table 2 in the frame of eq 4. In nondilute solutions, changes in local friction with changing polymer concentration can exert a significant influence on D. To account for the local friction, the D values presented in Table 2 were scaled by the ratio $\zeta(c)/\zeta(0) = (1 + \Phi)^2/(1 - \Phi)$, where Φ is the polymer volume fraction, in the way used and discussed by Wheeler and Lodge.[2] The logarithms of the corrected diffusion coefficients for the tracers in polyHEMA solutions were

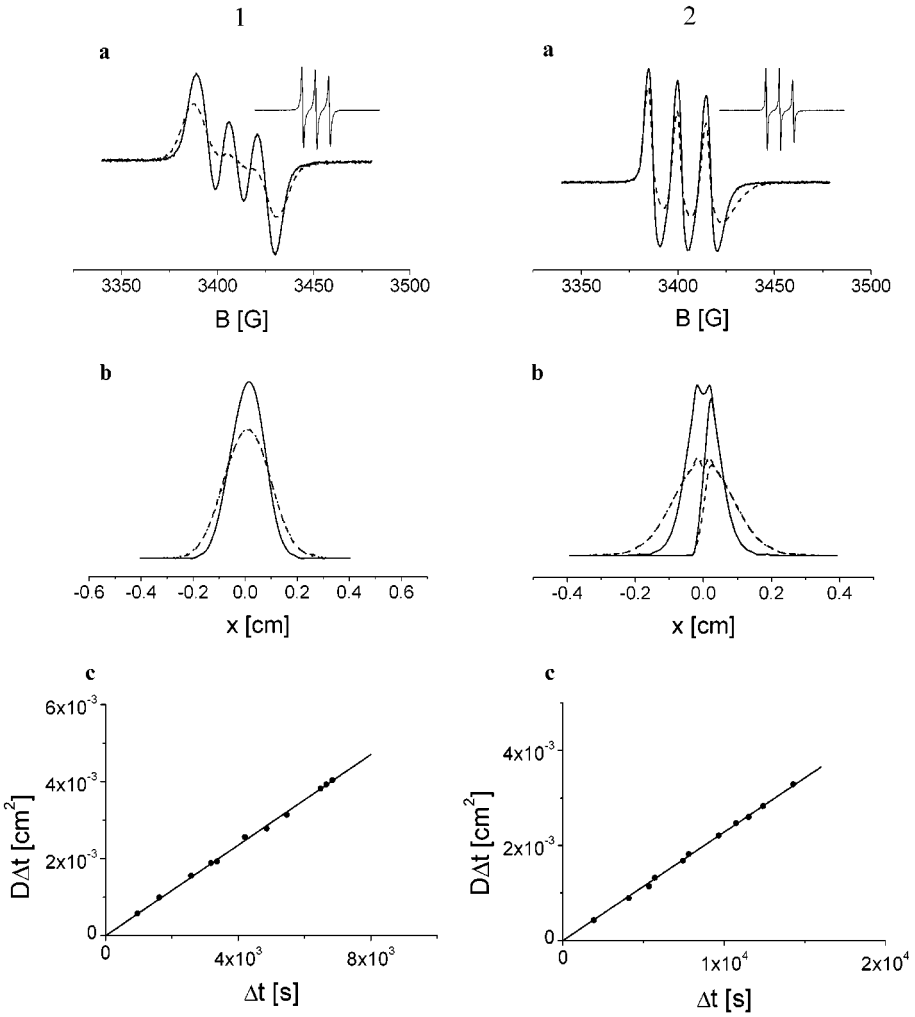

Figure 4. (a) Experimental ESRI profiles of tracer **VIa** measured in the presence of the magnetic field gradient G at time t_1 (full line) and t_2 (dashed line) after starting the diffusion and ESR spectrum of the sample without any magnetic field gradient present given in the inset for: Column 1: S30 polyHEMA methanolic solution using the "sandwich" arrangement at $G = 77.4$ G/cm, $t_1 = 35$ min, $t_2 = 88$ min. Column 2: S40 polyHEMA methanolic solution using the "from-top-to-bottom" arrangement at $G = 103.1$ G/cm, $t_1 = 66$ min, $t_2 = 258$ min. (b) Column 1: experimental concentration profiles of the tracer in the sample at times t_1 (full line) and t_2 (dashed line) determined by the deconvolution procedure and the fit of eq 5 to the profile determined at time t_2 with the diffusion coefficient $D_{1b} = 5.94 \times 10^{-7}$ cm^2/s (dotted line indistinguishable from the dashed line). Column 2: experimental concentration profiles of the tracer in the sample at time t_1 (full line) and t_2 (dashed line) determined by the deconvolution procedure and corresponding symmetrized profiles (see the text) and the perfect fit of eq 5 to the symmetrized profile determined at time t_2 with the diffusion coefficient $D_{2b} = 2.26 \times 10^{-7}$ cm^2/s (dotted line nearly indistinguishable from the dashed line). (c) Dependence of the values $D\Delta t$ on the time interval $\Delta t = t_2 - t_1$ for various initial−final concentration profile pairs; slope of the linear dependence determines the diffusion coefficient $D_{1c} = 5.88 \times 10^{-7}$ cm^2/s and $D_{2c} = 2.28 \times 10^{-7}$ cm^2/s.

Table 2. Diffusion Coefficients of Paramagnetic Tracers in Polymer Solutions and Gels (in 10^{-8} cm^2/s)

		tracer/M_w							
		IV 186		**V** 230		**VIa** 1840		**VIb** 2920	
sample code	c^a (g/mL)	D	$D_{corr}{}^b$	D	$D_{corr}{}^b$	D	$D_{corr}{}^b$	D	$D_{corr}{}^b$
G23	0.201	240	380	100	160	29	46	31	50
G29	0.255					16	29	8.8	16
G35	0.323	120	250	63	130	6.6	14	5.5	11
S15	0.126	797	1070	612	820	164	220	107	144
S20	0.171	642	954	448	666	144	214		
S23	0.199	591	936			95.7	152	67.9	108
S30	0.268	451	837	266	494	57.9	107	39.0	72.4
S35	0.319	347	724	210	438	36.5	76.1	25.2	52.6
S36	0.330	325	695	177	379	35.8	76.6	19.8	42.4
S40	0.373	244	576	127	300	25.6	60.5	12.7	30.0
S45	0.429	168	453	89.8	242	15.9	42.8	8.23	22.2

[a] Polymer concentration. [b] Values corrected for local solvent friction in the matrix (see the text).

plotted in Figure 5 versus the reciprocal hydrodynamic correlation length ξ_H determined for the solution matrices by DLS. The ξ_H values for concentrations of polyHEMA in methanolic solutions used in ESRI experiments were determined by splining the concentration dependence presented in Table 1 with a polynomial

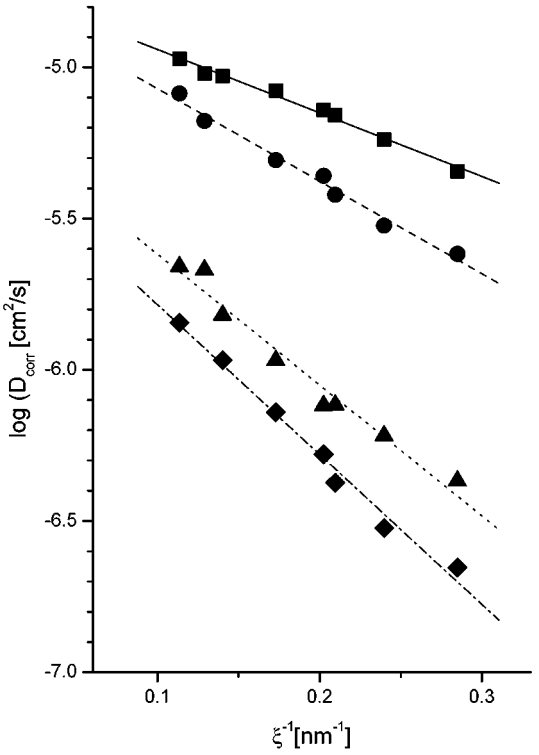

Figure 5. Dependence of the corrected diffusion coefficients of tracers (■, **IV**; ●, **V**; ▲, **VIa**; ♦, **VIb**) in methanolic solutions of polyHEMA containing entangled polymer chains on the reciprocal hydrodynamic screening length determined by DLS. The lines represent the best linear fits to the experimental data.

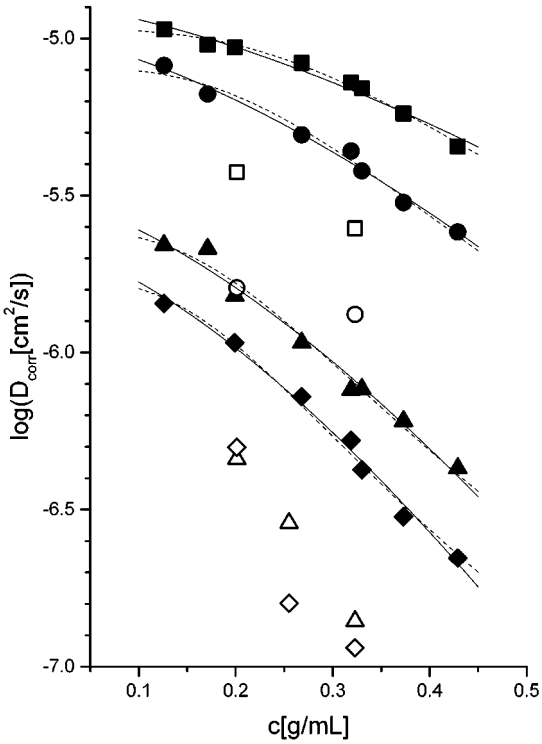

Figure 6. Dependence of the corrected diffusion coefficients of the tracers on the polymer concentration in methanolic solutions of polyHEMA containing entangled polymer chains (solid symbols; see Figure 5 for explanation) and in HEMA gels equilibrium-swollen with methanol (open symbols). Best fits to the data for a particular tracer in concentrated solutions calculated using Phillies' (eq 2) and Petit's (eq 3) models, and the parameters presented in Table 3 are given by solid and dashed lines, respectively.

of the fifth order and calculating correlation lengths for the concentrations required. It follows from Figure 5 that eq 4 fits the data measured in concentrated polyHEMA methanolic solutions very well. The slope of presented linear fits to the experimental data in the log D vs ξ_H^{-1} coordinates increases with increasing size of the paramagnetic tracer as eq 4 predicts giving the R values equal to 2.1, 3.1, 4.3, and 5.0 nm for tracers **IV**, **V**, **VIa**, and **VIb**, respectively. Masaro et al.[5] determined R_H for PEGs in the range of molecular weights from monomer up to 4626 in water at 23 °C using the Stokes−Einstein equation and diffusion coefficients determined by the PGSE technique. Among others they found $R_H = 20.59$ Å and $R_H = 22.69$ Å for M_w equal to 1532 and 2246, respectively. Static light scattering experiments performed by Zhu and Brown[3] showed that R_G of high-molecular-weight PEGs (M_w ranging from 145 000 to 1 200 000) in methanol at 25 °C follows the power dependence $R_G = 0.16\ M_w^{0.585}$ Å (which gives $R_G \sim 1.2$ nm and $R_G \sim 1.6$ nm for M_w equal to 1500 and 2500, respectively). The presence of terminal nitroxides is probably responsible for the higher dimensions of the **VIa** and **VIb** tracers compared with dimensions of comparable PEGs without any paramagnetic end groups.

The dependence of the corrected diffusion coefficients of the tracers on the polyHEMA concentration in methanolic solution, which was in all the matrixes presented in Table 2 well above c^*, was analyzed in the frame of the Phillies' and Petit's models mentioned above. Equations 2 and 3 were fitted to the data presented in Table 2. For each of the models the concentration dependences of the diffusion coefficients of all four tracers were fitted simultaneously using D_0, α, and ν as variable parameters but keeping ν, which

Table 3. Best Fit Parameters of Phillies' and Petit's Models to the Experimental Concentration Dependence of Diffusion Coefficients of the Paramagnetic Tracers in PolyHEMA Methanolic Solutions

	Phillies' model: $D = D_0 \exp(-\alpha_2 c^{\nu_2})$			Petit's model: $D = D_0/(1 + \alpha_3 c^{2\nu_3})$		
tracer	D_0 (10^{-6} cm²/s)	α_2	ν_2	D_0 (10^{-6} cm²/s)	α_3	ν_3
IV	13	3.4	1.48	11	18	1.54
V	10	5.0	1.48	8.1	33	1.54
VIa	3.1	7.2	1.48	2.5	68	1.54
VIb	2.2	8.2	1.48	1.7	89	1.54

according to the theoretical prediction characterizes the matrix, the same for each model. Both models fit the experimental data well at a similar level of accuracy (Figure 6). A similar conclusion was drawn on the basis of results presented for diffusion of PEG 600 in aqueous PVA solutions and in some water-swollen gels.[3] The best fit parameters are presented in Table 3. Those concerning diffusion of tracers **VIa** and **VIb** can be compared with the parameters characterizing the concentration dependence of diffusion of PEG 600, 1500, 2000, and 4000 in the above-mentioned PVA−water systems.[3,5] The best fit values for D_0 decreasing with increasing M_w of the tracer and close to the published data[3,5] were found for both mentioned models in agreement with theoretical predictions. More than twice higher values for parameters ν_2 and ν_3 were found in this study when compared with both theoretical predictions and values determined for the PVA−water system. When trying to explain such difference, we have to realize first of all that the values of these parameters are expected to

depend on the solvent quality, which is much poorer for our polyHEMA−methanol system than for PVA−water. In the case of Phillies' model, the α_2 values increasing with the M_w of the tracer and higher than the values published[10] for PEG 600 ($\alpha_2 = 3.5-4.5$ for various matrices) were found for both PEGs in this study. For the $k\beta^2$ parameter of Petit's model values (calculated as D_0/α_3) decreasing with the M_w of the tracer similarly to the published data[2] but lower (0.04 and 0.02 $\times 10^{-10}$ m^2/s for tracers **VIa** and **VIb**, respectively) were found. According to theoretical predictions, β should be a constant independent of properties of the matrix, and the jump frequency k should vary with molecular weight or the size of the tracer and with the size of the cavities in the polymer−solvent system between which the tracer is assumed to jump. Regarding the poorer quality of methanol for polyHEMA compared with water as solvent for PVA, lower dimensions of the cavities and lower values of the $k\beta^2$ parameter could be expected in our case.

Diffusion coefficients of the tracers measured in HEMA gels corrected in the same way as those measured in solutions are presented in Figure 6 for comparison. Slower diffusion coefficients measured in HEMA gels compared with polyHEMA solutions in matrices with the same polymer concentration follow from Figure 6. There exist at least two reasons for the observed difference. First, in cross-linked gel matrixes permanent cross-links are present in addition to temporary entanglement points. The presence of additional permanent cross-links is clearly demonstrated by smaller ξ_H found in HEMA gels when compared with polyHEMA solutions at the same polymer concentration (Table 1). This effect is particularly visible in the case of more cross-linked gels G29 and G35 because the concentration of permanent cross-links should be proportional to the cross-linker concentration, at least in a certain range of low cross-linker concentrations. Permanent cross-links in gels are additional topological constraints, which could slow down the tracer diffusion. In lightly cross-linked gel G23 ($c = 0.201$ g/mL), only minor differences in hydrodynamic correlation lengths were measured compared with solution S23. Nevertheless, practically the same relative decrease in diffusion coefficients for all four tracers was observed when comparing both mentioned matrixes. This seems to indicate that not only absolute concentration of the temporary and permanent cross-links in the matrix but also their ratio could affect the ratio of diffusion coefficients of tracers. In other words, shortening of the hydrodynamic correlation length in the gels due to the presence of permanent cross-links cannot explain quantitatively the observed decrease in the tracer diffusion coefficients. The diffusion coefficient of the tracer in a matrix characterized by a particular hydrodynamic correlation length seems to depend on the proportion of permanent cross-links present in the matrix. Second, the presence of permanent cross-links in gels probably also affects the local friction in a way that is not properly accounted for by the above-mentioned correction for the local friction.

Conclusions

Suitable experimental arrangements of ESRI experiments aimed at determination of diffusion coefficients characterizing macroscopic translational diffusion of paramagnetic tracers in polymer solutions and gels were selected by comparison of several sample configurations. Methods of treatment of experimental data based on mathematical deconvolution and fitting procedures were elaborated. Diffusion coefficients for four paramagnetic tracers in nondilute solutions of polyHEMA in methanol and in HEMA gels equilibrium-swollen with methanol were determined. Both solution and gel matrices were characterized by a hydrodynamic correlation length measured by the DLS technique. Diffusion coefficients were found to decrease with increasing molecular weight of the tracer in all the matrices studied. The dependences of the corrected diffusion coefficients on the polyHEMA concentration in methanolic solutions were well fitted within the frame of both Phillies' and Petit's models on approximately the same level of accuracy. The best fit values of characteristic parameters for each of the models were compared with both theoretical predictions and published experimental values. Lower values of diffusion coefficients of all four tracers were found in HEMA gels compared with a polymer solution containing the same concentration of the polymer. The data found indicate that slowing down the diffusion of the tracers in gels depends not only on the presence of additional permanent cross-links demonstrated by shortening hydrodynamic screening length of the matrix but also on the character of the obstacles (temporarily entanglements vs permanent cross-links) as well. Experiments on similar systems are in progress to provide more reliable data, in particular on gel matrices.

Acknowledgment. This research was supported by the Grant Agency of the Academy of Sciences of the Czech Republic (Project AVOZ4050913) and by the Polymers Program of the National Science Foundation, U.S.A. A.M. is thankful for hospitality and support at UDM when performing ESRI measurements. We thank Dr. J. Horský for performing and interpreting MALDI−TOF measurements, Dr. J. Stejskal and Mrs. M. Němcová for static light scattering, Dr. P. Holler for gel chromatography, and Dr. P. Štěpánek (all IMC Prague) for stimulating discussions.

References and Notes

(1) Phillies, G. D. J. *J. Phys. Chem.* **1989**, *93*, 5029.
(2) Wheeler, L. M.; Lodge, T. P. *Macromolecules* **1989**, *22*, 3399 and references cited therein.
(3) Masaro, L.; Ousalem, M.; Baille, W. E.; Lessard, D.; Zhu, X. X. *Macromolecules* **1999**, *32*, 4375.
(4) Devanand, K.; Selser, J. C. *Macromolecules* **1991**, *24*, 5943.
(5) Masaro, L.; Zhu, X. X.; Macdonald, P. M. *Macromolecules* **1998**, *31*, 3880.
(6) Zhou, P.; Brown, W. *Macromolecules* **1990**, *23*, 1131.
(7) Waggoner, R. A.; Blum, F. D.; Lang, J. C. *Macromolecules* **1995**, *28*, 2658.
(8) Flory, P. J. *Principles of Polymer Chemistry*; Cornell University Press: Ithaca, NY, 1953.
(9) de Gennes, P. G. *Scaling Concepts in Polymer Physics*; Cornell University: Ithaca, NY, 1979.
(10) Petit, J.-M.; Zhu, X. X.; Macdonald, P. M. *Macromolecules* **1996**, *29*, 70.
(11) Petit, J.-M.; Roux, B.; Zhu, X. X.; Macdonald, P. M. *Macromolecules* **1996**, *29*, 6031.
(12) Matsukawa, S.; Ando, I. *Macromolecules* **1996**, *29*, 7136; (b) **1997**, *30*, 8310; (c) **1999**, *32*, 1865.
(13) Ong, C. J.; Saxon, R. *J. Appl. Polym. Sci.* **1976**, *20*, 1695.
(14) *EPR Imaging and in Vivo EPR*; Eaton, G. R., Eaton, S. S., Ohno, K., Eds.; CRC Press: Boca Raton, FL, 1991.
(15) Moscicki, J. K.; Shin, Y.-K.; Freed, J. H. *J. Magn. Reson.* **1989**, *84*, 554.
(16) Moscicki, J. K.; Shin, Y.-K.; Freed, J. H. *J. Chem. Phys.* **1993**, *99*, 634.
(17) Xu, D.; Hall, E.; Ober, Ch. K.; Moscicki, J. K.; Freed, J. H. *J. Phys. Chem.* **1996**, *100*, 15856.

(18) Degtyarev, Y. N.; Schlick, S. *Langmuir* **1999**, *15*, 5040.
(19) Schlick, S.; Pilař, J.; Kweon, S.-C.; Vacík, J.; Gao, Z.; Labský, J. *Macromolecules* **1995**, *28*, 5780.
(20) Gao, Z.; Pilař, J.; Schlick, S. *J. Phys. Chem.* **1996**, *100*, 8430.
(21) Schlick, S.; Eagle, P.; Kruczala, K.; Pilař, J. In *Spatially Resolved Magnetic Resonance: Methods, Materials, Medicine, Biology, Rheology, Ecology, Hardware*; Blümler, P., Blümich, B., Botto, R., Fukushima, E., Eds.; Wiley-VCH: Weinheim, Germany, 1998; Chapter 17, p 221.
(22) Pilař, J.; Labský, J.; Marek, A.; Koňák, È.; Schlick, S. *Macromolecules* **1999**, *32*, 8230.
(23) Jakeš, J. *Collect. Czech. Chem. Commun.* **1995**, *60*, 1781.
(24) Štěpánek, P. In *Dynamic Light Scattering: The Method and Some Applications*; Brown, W., Ed.; Oxford University Press: New York, 1993.
(25) Vink, H. *J. Chem. Soc., Faraday Trans. 1* **1985**, *81*, 1725.
(26) Vošický, V.; Bohdanecký, M.; Dušek, K. *Collect. Czech. Chem. Commun.* **1977**, *42*, 1627.
(27) Geisler, E. In *Dynamic Light Scattering: The Method and Some Applications*; Brown, W., Ed.; Oxford University Press: New York, 1993.
(28) Hornak, J. P.; Moscicki, J. K.; Schneider, D. J.; Freed, J. H. *J. Phys. Chem.* **1986**, *84*, 3391.
(29) Jansson, P. A. *Deconvolution with Applications in Spectroscopy*; Academic Press: London, 1984; Chapter: *Traditional Linear Deconvolution Methods*; (b) Chapter: *Modern Constrained Nonlinear Methods.*
(30) *Matlab Signal Processing Toolbox User's Guide Version 4.0*; The MathWorks: Natick, MA, 1996.
(31) Howard, S. J. *Fourier Spectrum Continuation* and *Minimum-Negativity-Constrained Fourier Spectrum Continuation*. In *Deconvolution With Applications in Spectroscopy*; Jansson, P. A., Ed.; Academic Press: London, 1984.
(32) Howard, S. J. *J. Opt. Soc. Am. A* **1981**, *71*, 95.
(33) Howard, S. J. *J. Opt. Soc. Am. B* **1981**, *71*, 819.
(34) Reinsch, C. *Numer. Math.* **1967**, *10*, 177.
(35) Frieden, B. R. *Restoring with Maximum Likelihood*; Technical Report No. 67; Optical Sciences Center, University of Arizona: Tucson, 1971.
(36) Crank, J. *The Mathematics of Diffusion*; Clarendon Press: Oxford, UK, 1993.
(37) Aharoni, S. M. *J. Macromol. Sci., Phys.* **1978**, *15*, 347.
(38) Adam, M.; Delsanti, M. *Macromolecules* **1978**, *10*, 1229.

MA0200874